JOURNAL OF Materials CHEMISTRY
Feature Article

Aluminosilicate mesostructures with improved acidity and hydrothermal stability†

Yu Liu and Thomas J. Pinnavaia*

Department of Chemistry, Michigan State University, East Lansing, MI 48824, USA. E-mail: pinnavai@cem.msu.edu.

Received 29th April 2002, Accepted 4th July 2002
First published as an Advance Article on the web 3rd October 2002

Significant improvements in both the hydrothermal stability and the acidity of mesostructured aluminosilcates have been reported recently. New assembly pathways, along with post-synthesis treatment methods, have made it possible to form structures with thick and more highly crosslinked framework walls. The resulting structures are slow to degrade under hydrothermal conditions in comparison to conventional analogs. Also, improved methodologies for grafting Al centers into the walls of pre-assembled frameworks have afforded aluminosilicate mesostructures with enhanced acidity. The most promising strategy for improving the hydrothermal stability and acidity of aluminosilicate mesostructures, however, is based on the use of protozeolitic nanoclusters. These so-called "zeolite seeds" can be directly assembled into hexagonal, cubic, wormhole, and foamlike framework structures under a variety of assembly conditions. They also can be grafted into the walls of pre-assembled frameworks to form more stable acidic derivatives.

1 Introduction

Mesoporous molecular sieves with well-defined pore sizes of 2 to 50 nm have received much attention in the last decade. Different assembly pathways have been developed for the synthesis of hexagonal (MCM-41),[1–8] cubic (MCM-48),[9–11] wormhole (HMS, MSU-X),[12–27] lamellar-vesicular (MSU-G),[28,29] 2D hexagonal (SBA-15, MSU-H),[30–35] and foamlike (MCF, MSU-F)[35–39] mesoporous materials. In particular, mesostructured aluminosilicate compositions have been the focus of many recent studies, because these materials have potential applications in catalysis and adsorption technology, particularly for use as acid catalysts for bulk hydrocarbon conversion.

In comparison to microporous zeolites, ordered mesoporous materials overcome the pore size constraint of zeolites and allow the more facile diffusion of bulk molecules. These are properties that are highly desirable for potential applications in FCC (fluid catalytic cracking) processes and chemical conversions in condensed media. However, the acidity and hydrothermal stability of mesostructured aluminosilicates are less than required for many catalytic applications. The instability of these structures has been attributed in part to the thinness and incomplete crosslinking of the pore walls.[40]

Since hydrothermal stability and acidity are essential for the application of the mesoporous materials in catalysis, several approaches have aimed at improving these properties. The strategies that have been investigated include (i) decreasing the silianol group content of the framework by silylation of the surface –OH groups in order to make the surface more hydrophobic and thereby improve the stability in water,[41–43] (ii) thickening the walls of MCM-41 by post-treatment of primary MCM-41 to improve the hydrothermal stability, and subsequently grafting Al centers into the framework walls,[44–49] (iii) adding salts to synthesis gels to facilitate the condensation of silanol groups during the formation of the framework,[50] thereby improving framework crosslinking, (iv) partially transforming the walls into a pentasil zeolite phase by post-synthesis treatment of the original mesoporous aluminosilicate with zeolite structure-directing agents, such as tetrapropylammonium salts,[51,52] (v) generating microporous zeolite–mesostructure composite mixtures to improve both hydrothermal stability and acidity,[53–55] (vi) using triblock copolymer surfactants to make thick wall mesoporous structures such as SBA-15,[30–35] and (vii) using neutral Gemini amine surfactants to make thick-walled, vesicle-like lamellar frameworks with improved hydrothermal stability.[28,29]

In general, the above approaches certainly improve the stability in comparison to the originally reported M41S materials. Nevertheless, the acidity and hydrothermal stability of mesostructured aluminosilicates remain much lower than those of crystalline microporous zeolites. In particular, the steam stability at 800 °C is still poor, thus hindering the potential commercial application of these materials.

A recent breakthrough in improving both the hydrothermal stability and acidity of mesoporous aluminosilicates has been made through the use of nanoclustered zeolite seeds as framework precursors.[56–60] These protozeolitic precursors contain subunits of the zeolite structures that they nucleate. This approach was first demonstrated using faujasitic zeolite (FAU) seeds to assemble a steam-stable hexagonal MCM-41 analog.[56] Shortly afterwards, additional studies successfully assembled steam-stable and strongly acidic hexagonal MCM-41 derivatives (denoted MSU-S and MAS-5) by using ZSM-5 (MFI) and Beta (BEA) zeolite seeds as precursors.[56–60] The idea of using zeolite seeds as precursors to assemble steam-stable and strongly acidic large pore materials has been extended more recently to include hexagonal SBA-15 analogs, denoted MSU-S/H and MAS-7.[58,61] Also, strongly acidic mesostructured cellular foam (MCF) analogs, denoted MSU-S/F, have been assembled using ZSM-5, Beta, and faujasitic zeolite seeds at pH <2–6.5.[58]

This review summarizes the more promising strategies for improving further the hydrothermal stability and acidity of mesoporous aluminosilicates. Particular attention is given to approaches that lead to the assembly of thick-wall silica structures and post-synthesis techniques for introducing tetrahedral AlO_4 units into the framework to enhance acidity. In addition, the use of protozeolitic seeds to directly assemble hydrothermally stable and strongly acidic aluminosilicate mesostructures is discussed in detail.

†Basis of a presentation given at Materials Discussion No. 5, 22–25 September 2002, Madrid, Spain.

DOI: 10.1039/b204094h

2 Thick-walled mesostructures

2.1 Triblock copolymer templating of SBA-15

In the original synthesis of MCM-41 and related M41S-type materials, surfactant molecules with small, ionic hydrophilic head groups and hydrophobic alkyl tails were used to template ordered arrays of mesoporous silica. If no pore expanding agents (such as trimethylbenzene) were added, the pore size of these materials was around 2.0–4.0 nm and the wall thickness was between 1 and 2 nm. The poor hydrothermal stability of this mesostructure was quickly recognized and attributed to the thin, amorphous wall structure. In 1998, Stucky *et al.* successfully synthesized a thick-walled 2D hexagonal mesoporous material (denoted SBA-15) by using a triblock copolymer, polyethylene oxide–polypropylene oxide–polyethylene oxide (PEO–PPO–PEO), as a structure director under strongly acidic assembly conditions.[30] SBA-15 exhibited a wall thickness between 3 and 7 nm and large pore sizes of 7–12 nm. The thick wall of SBA-15 imparted significantly greater hydrothermal stability in comparison to conventional MCM-41. No structural degradation of SBA-15 was observed after heating in boiling water for 24 h.

Soon afterwards, Yue *et al.*[62] synthesized Al-SBA-15 by direct synthesis and investigated the hydrothermal stability and acidity of this product. As shown in Fig. 1, Al-SBA-15 showed better steam stability in comparison to Al-MCM-41. In addition, as shown by the XRD patterns in Fig. 1, Al-SBA-15 was stable under both acidic (pH 2) and basic (pH 11) conditions. Finally, Al-SBA-15 showed good activity for cumene cracking. It should be noted, however, that the temperature used to test steam stability (550 °C), was lower than the temperature normally used in commercial processes for regenerating zeolites (*ca.* 800 °C). We will show later that the steam stability of Al-SBA-15 is comparatively poor at 800 °C.

2.2 Gemini amine surfactant templating of MSU-G

As the first examples of stable mesoporous lamellar silicas with a vesicular hierarchical structure, MSU-G silicas were successfully synthesized using Gemini amine surfactants.[28] In contrast to MCM-41, which was assembled through an electrostatic pathway involving a cationic surfactant and an anionic precursor, MSU-G was prepared *via* an electrically neutral, H-bonded pathway. A comparison of the structural stability of MSU-G thermal (1000 °C) and hydrothermal treatment (boiling H_2O) in comparison to MCM-41, KIT-1, and SBA-3 is provided by the XRD patterns shown in Fig. 2. Table 1 summarizes the textural properties of MSU-G, MCM-41, and KIT-1 after the same thermal and hydrothermal treatments. Upon calcination at 1000 °C for 4 h, MSU-G retained 75% of its initial pore volume and pore size, as well as 90% of its surface area. Hydrothermal treatment in boiling water for 56 h had a negligible effect on the framework porosity of MSU-G, as confirmed by XRD and N_2 sorption isotherms. In comparison to MSU-G, as well as SBA-15, previously reported KIT-1, SBA-3, and MCM-41 mesostructured silicas exhibited

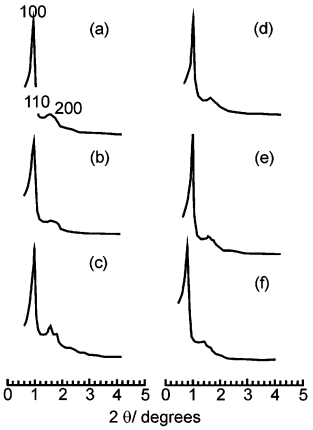

Fig. 1 XRD patterns of (a) Al-SBA calcined at 550 °C and the same sample after (b) calcination at 800 °C, (c) steaming at 550 °C, (d) exposure to aqueous acid at pH 2, (e) exposure to water, and (f) exposure to aqueous base at pH 11. Reproduced from ref. 62 by permission of The Royal Society of Chemistry.

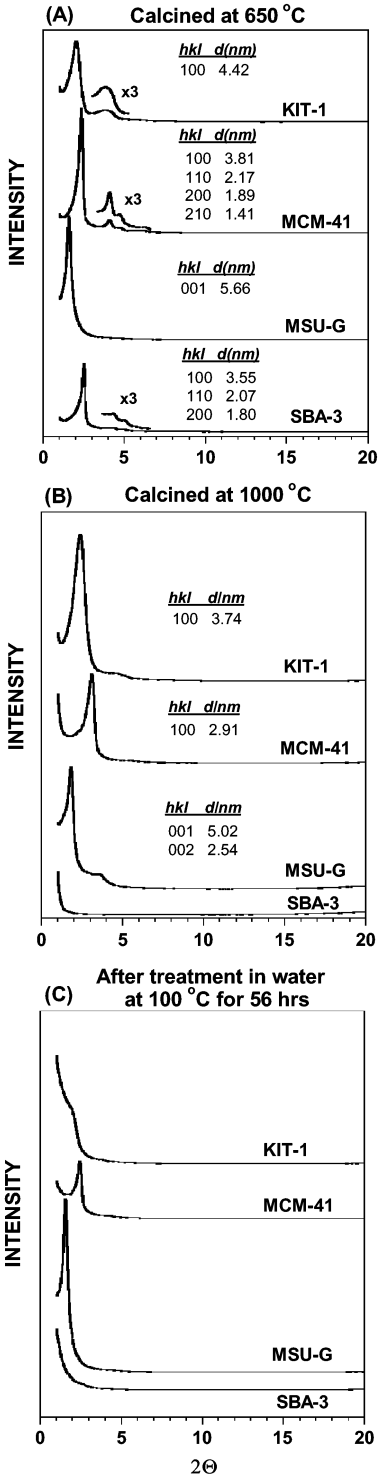

Fig. 2 XRD patterns for MSU-G, SBA-3, MCM-41, and KIT-1 silicas after (A) calcination at 650 °C, (B) calcination at 1000 °C, and (C) exposure to boiling water for 56 h. Note that the crystallinity of SBA-3 is completely lost after calcination at 1000 °C and after exposure to boiling water for 56 h. Reproduced from ref. 28 by permission of Elsevier.

Table 1 Structural properties of MCM-41, KIT, and MSU-G molecular sieve silicas after thermal and hydrothermal treatments. Reproduced from ref. 28 by permission of Elsevier

	Surface area/m^2 g^{-1}			Pore volume/cm^3 g^{-1}			HK pore size/Å		
Treatment	MCM-41	KIT-1	MSU-G	MCM-41	KIT-1	MSU-G	MCM-41	KIT-1	MSU-G
Calcined at 1000 °C	134 (12%)	725 (68%)	370 (90%)	0.07 (8%)	0.35 (36%)	0.31 (74%)	—	25 (66%)	24 (75%)
Calcination at 650 °C and hydrothermal treatment at 100 °C for 56 h	245 (21%)	477 (45%)	407 (99%)	0.54 (62%)	0.59 (61%)	0.38 (90%)	—	—	32 (100%)

comparatively poor hydrothermal stability. The framework structures were almost completely sacrificed in boiling water after 56 h.

It is clear that the improved hydrothermal stability of MSU-G, like SBA-15, is attributable in large part to the thicker framework walls (2.5 nm) in comparison to MCM-41, KIT-1, and SBA-3. This same structural feature is expected to contribute to the stability of aluminum-substituted derivatives. Another notable feature associated with the higher hydrothermal stability of MSU-G was the higher Q^4/Q^3 ratio (6.2) for the framework SiO_4 units. Normally, as-synthesized mesoporous silicates have Q^4/Q^3 ratios less than 2.0 and calcined forms have ratios less than 3.0. The higher Q^4/Q^3 value for MSU-G means that the framework walls are more completely crosslinked and probably more hydrophobic than other mesostructured silicates. These features contribute substantially to the improved hydrothermal stability. In general, as-prepared silica mesostructures assembled through electrically neutral assembly pathways are more highly crosslinked than mesostructures prepared *via* an electrostatic charge matching mechanism.

The reactivity of Al-MSU-G as an acid catalyst for flavan synthesis in an organic solvent has been investigated in comparison to Al-MCM-41. As shown in Table 2, the yield provided by Al-MSU-G is substantially higher than that obtained for Al-MCM-41 or sulfuric acid. It was concluded that the enhanced reactivity was a result of a comparatively short pore length and the more facile access of the reagents to the acidic sites on the framework walls.

3 Post-synthesis treatment methods for improved stability

3.1 Restructuring of MCM-41

In an effort to increase the wall thickness and crosslinking of MCM-41, Mokaya employed calcined MCM-41 as the silica source for the secondary synthesis of the same mesostructure.[63] He also prolonged the synthesis time of MCM-41.[49] Upon secondary synthesis, the restructured MCM-41 silica exhibited improved long-range structural ordering and a marked increase in hydrothermal stability. Basically, the improved hydrothermal stability was attributed to the increased pore wall thickness by secondary synthesis. Moreover, after post-synthesis grafting of Al centers onto the framework walls of the secondary silica MCM-41, both the hydrothermal stability and acidity were significantly improved.[45] As shown in Fig. 3 and 4, the Al-grafted secondary MCM-41, denoted CAH5 (Si/Al = 6.1) and CAP10 (Si/Al = 9.8), exhibited well-resolved higher order (110), (210), and (200) peaks after boiling in water for 150 h. There were no significant changes in *d* spacings. The N_2 isotherms of CAH5 and CAP10 were substantially changed, however. In comparison to the freshly calcined CAH5 and CAP10, the mesostructures exposed to boiling water for 150 h showed a broadening of the pore size distribution. Interestingly, hydrothermally treated CAH5 and CAP10 exhibited even higher cumene cracking activity (Table 3), which is potentially very important for commercial applications. It was concluded that the increased acidity of hydrothermally

Table 2 The catalytic activity of Al-substituted (2 mol%) MSU-G and MCM-41 materials for the alkylation of DTBP with cinnamyl alcohol.[a] Reproduced from ref. 28 by permission of Elsevier

Catalyst	Aluminum source	Conversion of DTBP (%)	Selectivity of flavan (%)	Yield of flavan (%)
Al-MCM-41	$Al(NO_3)_3$	50.4	61.9	31.2
Al-MSU-G	$Al(NO_3)_3$	76.2	64.1	48.8
Al-MSU-G	$Al(^iBuO)_3$	73.9	63.5	46.9
Al-MSU-G	$NaAlO_2$	69.1	65.3	45.1
H_2SO_4	—	25.5	36.9	9.4

[a]In a typical experiment, 250 mg of catalyst or 30 mg of H_2SO_4 was added to a solution of DTBP (1.0 mmol) and cinnamyl alcohol (1.0 mmol) in 50 ml of isooctane solvent at 90 °C.

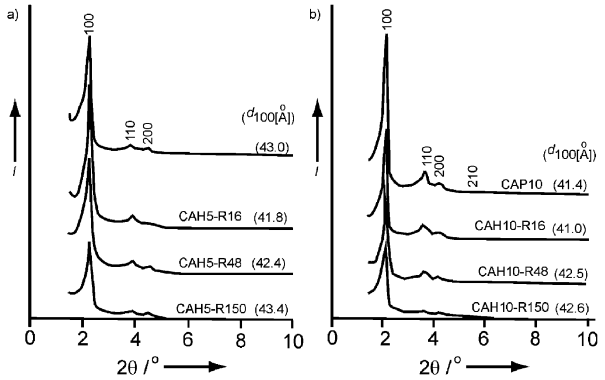

Fig. 3 X-Ray diffraction patterns of (a) "wet"-grafted CAH5 and (b) "dry"-grafted CAP10 mesoporous aluminosilicates before and after various hydrothermal treatments in boiling water. The R values indicate the time in hours that the sample was exposed to boiling water.Reproduced from ref. 45 by permission of Wiley-VCH.

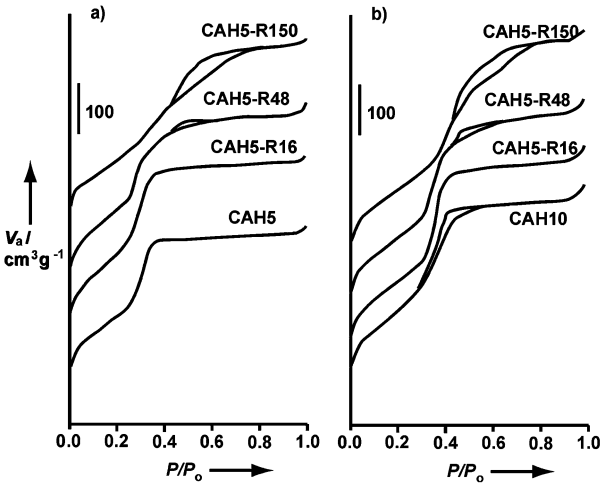

Fig. 4 N_2 sorption isotherms for (a) "wet"-grafted CAH5 and (b) "dry"-grafted CAP10 mesoporous aluminosilicates before and after various hydrothermal treatments in boiling water. Reproduced from ref. 45 by permission of Wiley-VCH.

Table 3 Elemental composition, textural properties, acidity, and catalytic acidity of Al-grafted materials before and after various hydrothermal treatments. Reproduced from ref. 45 by permission of Wiley-VCH

Sample	Si : Al	Surface area/m^2 g^{-1}	Pore volume/ cm^3 g^{-1}	APD[a]/Å	Wall thickness[b]	Acidity[c]	Cumene conversion[d]
CAH5	6.1 : 1	753	0.62	25.8	23.9	0.88	0.98
CAH5-R16	5.1 : 1	834	0.70	24.0	23.4	1.25	1.33
CAH5-R48	4.5 : 1	902	0.70	26.8	22.2	1.38	1.34
CAH5-R150	4.2 : 1	724	0.65	31.0	19.1	1.29	1.32
CAP10	9.8 : 1	850	0.76	30.9	16.9	0.63	0.64
CAP10-R16	8.1 : 1	894	0.81	31.0	16.3	1.18	1.29
CAP10-R48	7.1 : 1	864	0.80	32.5	16.6	1.28	1.32
CAP10-R150	6.5 : 1	810	0.77	33.7	15.5	1.30	1.36

[a]APD = average pore diameter (determined using BJH analysis of the desorption isotherm). [b]Wall thickness = unit cell parameter (a_o) − APD, where a_o was obtained form the XRD data using the formula $a_o = 2d_{100}/\sqrt{3}$. [c]Given in mmol of H^+ per gram of sample. [d]Cumene cracking rate, in mmol per gram of catalyst per hour, after 20 min on stream. Total conversion equals a rate of 1.52. Under similar conditions, the conversion rate over ultrastable Y zeolite (CBV 740, Si : Al = 21 : 1) and HY zeolite (Si : Al = 3.6 : 1) was 1.34 and 0.54, respectively.

treated CAH5 and CAP10 was due to an increase in the Al/Si ratio in the framework. The increase in Al/Si ratio of CAH5 and CAP10 was attributed to the dissolution of non-framework silica during the hydrothermal treatment. Consistent with elemental analysis, an increase in the Al concentration on the framework walls was observed by XPS analysis. ^{27}Al NMR also was used to verify the dealumination of the hydrothermally treated framework. The amount of extra-framework Al increased with hydrolysis time.

The restructuring of primary MCM-41 to increase the wall thickness, followed by grafting with Al_{13} oligocations, was also reported to improve framework crosslinking.[49] Al-MCM-41 synthesized at 140 °C and a reaction time of 96 h exhibited the best hydrothermal stability, because these conditions afforded the thickest pore wall (2.2 nm). As shown in Fig. 5, the exposure of the resulting reaction product to 3% H_2O in N_2 at 800 and 900 °C for 4 h did not alter the XRD pattern. As indicated by the N_2 sorption isotherms, the sample steamed at 800 °C still exhibited a relatively sharp mesopore filling step. Upon steaming at 900 °C, 68% of the initial surface area and 50% of the initial pore volume was retained. Aside from a thicker pore wall, the framework crosslinking was higher than for conventional MCM-41, as indicated by ^{29}Si MAS NMR.

The above results showed that the hydrothermal stability of MCM-41 could be improved by restructuring the parent MCM-41 and grafting the framework with the Al_{13} oligocations of aluminum chlorhydrol. The improved hydrothermal stability was attributed to the combination of thicker pore walls and improved framework crosslinking upon Al grafting. More recently, it has been shown that sodium ions trapped in the framework walls of pure silica MCM-41 contribute substantially to the structural instability of the framework under hydrothermal conditions.[64] The sodium centers promote Si–O–Si bond cleavage that leads to the collapse of the mesostructure. Thus, the assembly of a silica mesostructure in the absence of sodium and the subsequent transformation of the pure silica mesostructure into an aluminosilicate derivative by grafting reaction with a sodium-free alumination agent should lead to a more stable product.

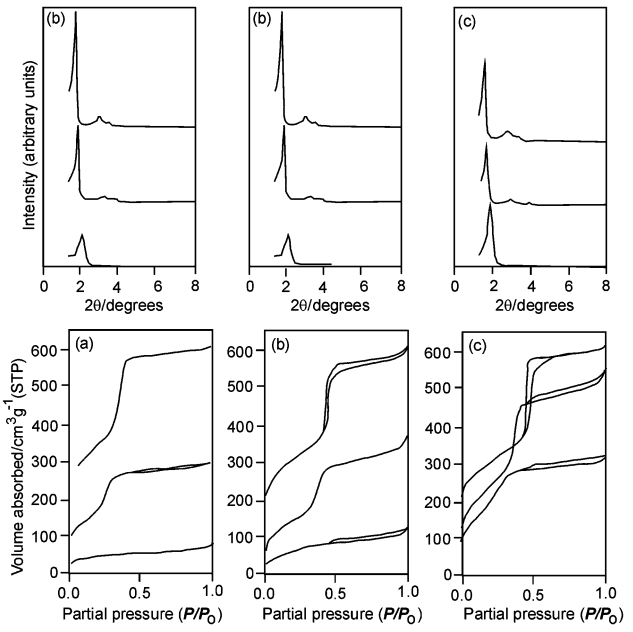

Fig. 5 XRD patterns and N_2 sorption isotherms for Al-grafted MCM-41 samples after calcination (top curves) and before and after hydrothermal treatments at 800 (middle curves) and 900 °C (bottom curves); the initial mesostructured silica precursors were assembled at (a) 150 °C, 48 h, (b) 140 °C, 96 h, and (c) 145 °C, 96 h. Reproduced from ref. 49 by permission of The Royal Society of Chemistry.

3.2 Partial transformation of framework walls into zeolitic nanocrystals

In comparison to crystalline microporous zeolites, mesoporous aluminosilicates lack hydrothermal stability and strong acidity due to their non-crystalline framework walls. Thus, several efforts to crystallize the walls of mesoporous aluminosilicate have been reported.

In 1997, van Bekkum *et al.*[65] first used the zeolite structure-directing agent tetrapropylammonium cation to treat Al-MCM-41 and Al-HMS mesostructures. The strategy was to improve the acidity of Al-MCM-41 and Al-HMS by partially recrystallizing the pore walls into nanosized ZSM-5. As shown in Table 4, the treated products, denoted PNA-1 and PNA-2, respectively, exhibited a substantial increase in cumene cracking activity. IR spectra (Fig. 6) provided evidence for the formation of ZSM-5 units. In contrast to the parent Al-MCM-41 and Al-HMS, the PNA samples afforded FTIR spectra with a distinct vibration at 550–600 cm^{-1}, indicative of the five-membered ring subunit of a pentasil zeolite. The

Table 4 Cumene conversion at 300 °C over PNAs and related parent materials. Reproduced from ref. 65 by permission of The Royal Society of Chemistry

	Cumene conversion (%) at time on stream	
Sample	10 min	3 h
MCM-41[a]	14.7	13.6
PNA-1	41.3	37.5
HMS[a]	24.8	26.8
PNA-2	47.6	42.4
ZSM-5[b]	95.1	93.7

[a]MCM-41 and HMS in the H^+-form. [b]H-ZSM-5 with Si/Al = 78.

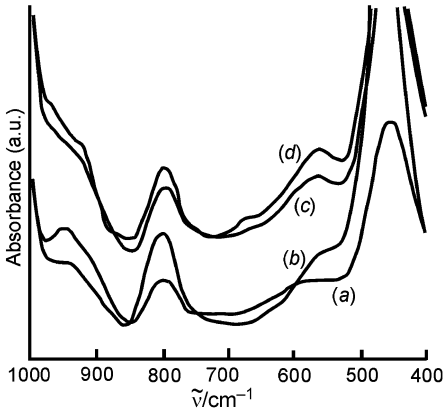

Fig. 6 FTIR adsorption spectra for (a) MCM-41, (b) PNA-1 prepared *via* treatment of MCM-41 with tetrapropylammonium cations, (c) HMS, and (d) PNA-2 obtained from treatment of HMS with tetrapropylammonium cations. Reproduced from ref. 65 by permission of The Royal Society of Chemistry.

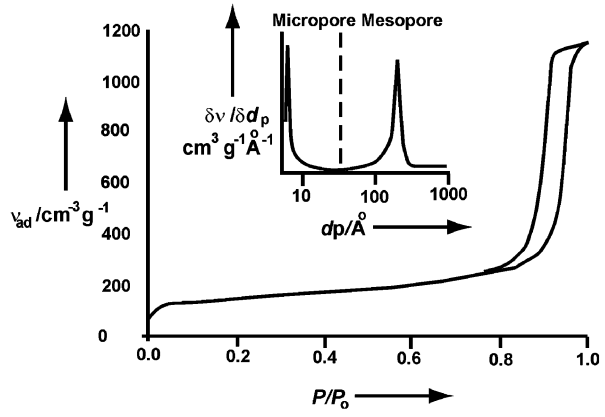

Fig. 8 N_2 sorption isotherms of UL-ZSM-5 after 2 days crystallization time. Inset: HK micropore and BJH mesopore distributions; d_p is the pore diameter. Reproduced from ref. 51 and 52 by permission of Wiley-VCH.

increase in acidity was attributed to the partial transformation of the amorphous aluminosilicate wall of MCM-41 and HMS into an embryonic ZSM-5 phase. No test of the hydrothermal stability was performed for the PNA samples.

It is unlikely that the framework wall of MCM-41 can be transformed to a crystalline zeolite phase while still maintaining the hexagonal MCM-41 mesostructure. The unit cell of ZSM-5 is around 2.5 nm, which is larger than the wall thickness of MCM-41. Clearly, once a zeolite phase is formed from MCM-41, it is likely to appear as a separated zeolite phase. This expectation was confirmed by more recent results from van Beckkum *et al.*[66] In the best case, the wall of MCM-41 was transformed into 3 nm ZSM-5 crystallites.

Following-up on van Beckkum's approach, Kaliaguine and co-workers[51,52] investigated the possibility of transforming a thicker wall MCF aluminosilicate into a crystalline zeolitic framework. As shown in Fig. 7, a ZSM-5 phase with 42% crystallinity was formed after hydrothermal treatment with tetrapropylammonium hydroxide. The N_2 isotherms for this material (denoted UL-ZSM-5), exhibited a typical type IV shape and a steep rise at low relative P/P_o, indicating the presence of both micropore and mesopore structures (Fig. 8). Further evidence for the presence of UL-ZSM-5 was provided by bright- and dark-field TEM images recorded on the same area of the sample. As shown in Fig. 9, the bright spots in the image correspond to ZSM-5 nanocrystals embedded in the particles of the mesostructure. The average size of the ZSM-5 nanocrystals was around 5 nm. ^{27}Al MAS NMR spectra exhibited a single resonance peak at a chemical shift of 54–58 ppm, which meant that all of the aluminum was tetrahedrally coordinated. The acidity of this material was determined by

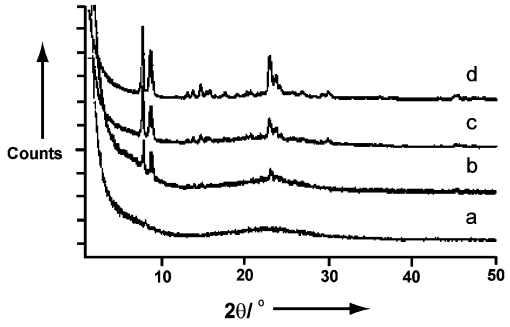

Fig. 7 XRD patterns of calcined UL-ZSM-5 reaction products (a) before crystallization and after crystallization times of (b) 1, (c) 2, and (d) 5 days. Reproduced from ref. 51 and 52 by permission of Wiley-VCH.

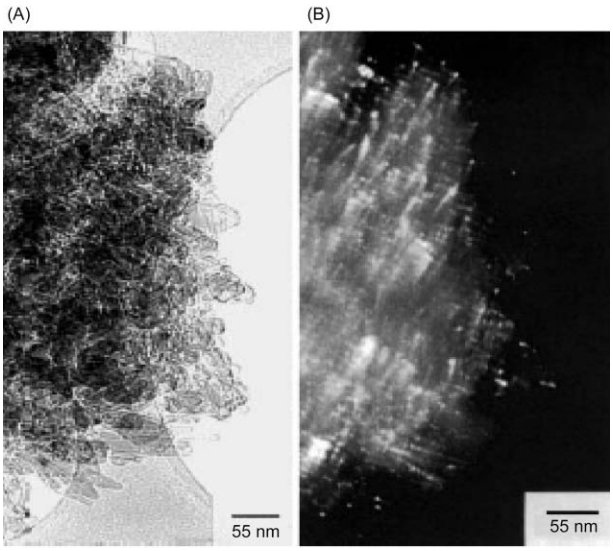

Fig. 9 Bright-field (A, left panel) and dark-field (B, right panel) TEM images of the same area of UL-ZSM-5 after 5 days crystallization time. Reproduced from ref. 51 and 52 by permission of Wiley-VCH.

pyridine adsorption and the results showed that the acidic strength was much stronger than the parent amorphous mesoporous material, as expected. No hydrothermal stability test was reported for this mixed-phase material.

In principle, the strategy of using thicker wall silica mesophases as precursors to nanophase microstructures is not limited to aluminosilicates. This approach has also been used to partially transform silica mesostructures into embedded nanoparticles of the microporous titanosilicate TS-1.[67]

4 Direct assembly and post-synthesis grafting using protozeolitic nanoclusters (zeolite seeds)

Soon after the discovery of mesoporous MCM-41 silicas, it was found that the incorporation of aluminum into the framework introduced mildly acidic functionality, as expected. At the same time, however, the direct incorporation of conventional aluminum precursors (*e.g.* sodium aluminate, aluminum alkoxides, Al_{13} oligomers) into the mesostructure generally compromised the long-range framework order, as well as the pore size distribution, particularly at aluminum substitution levels above *ca.* 8 mol%. More recently, however, we have shown that nanoclustered zeolite seeds, which are presumed to promote zeolite nucleation by adopting AlO_4 and SiO_4

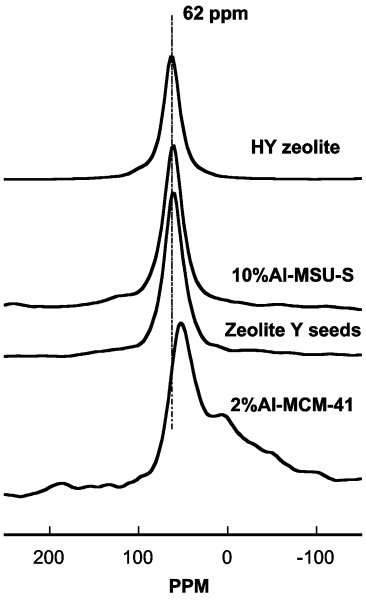

Fig. 10 ^{27}Al MAS NMR spectra of zeolite Y, calcined 10%Al-MSU-S, zeolite Y seeds, and calcined 2%Al-MCM-41.

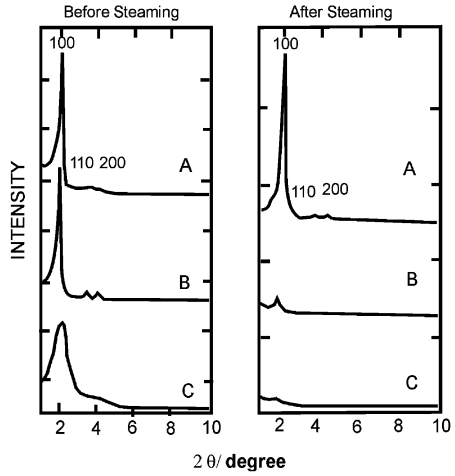

Fig. 11 XRD patterns of calcined (540 °C, 7 h) mesoporous aluminosilicate molecular sieves before and after steaming (800 °C, 5 h): (A) hexagonal 10%Al-MSU-S prepared from zeolite Y seeds; (B) "ultrastable" hexagonal 14%Al-MCM-41 prepared by grafting; (C) disordered 10%Al-MCM-41 prepared by direct synthesis from conventional silicate and aluminate precursors. Reproduced from ref. 56 by permission of The American Chemical Society.

tetrahedra connectivities that contain the secondary structural subunits of a crystallized zeolite, are ideally suited for assembling mesoporous aluminosilicates without compromising the long-range structural order. More importantly, the use of protozeolitic seeds in the assembly process also greatly improves hydrothermal stability and acidity.

4.1 Assembly of MSU-S from faujasitic zeolite seeds

The first steam-stable hexagonal mesoporous aluminosilicates were successfully assembled from faujasitic-type Y zeolite seeds.[56] Nanoclustered zeolite Y seeds were prepared by reacting sodium hydroxide, sodium aluminate, and sodium silicate under vigorous stirring at 100 °C overnight. ^{27}Al NMR of the seed mixture indicated the exclusive presence of tetrahedral aluminum at a chemical shift of 60–62 ppm (Fig. 10), which is consistent with the chemical shift of ^{27}Al in the subunits of zeolite Y. However, XRD patterns of the seed solution in thin film form showed no Bragg peaks, which indicated the absence of a well-crystallized zeolite Y phase. The assembly of a hexagonal mesostructure was achieved by lowering the pH of the seed solution to a value of about 9.0 and introducing cetyltrimethylammonium bromide (CTAB) as the structure director. The aluminum loading in the final mesostructures was controlled by the composition of the original seed solution (10–35 mol% Al). The steam-stable mesoporous aluminosilicate (denoted MSU-S) was obtained by exchanging the as-synthesized structure with NH_4NO_3 and then calcining at 540 °C for 7 h. Fig. 11 shows the XRD patterns of calcined 10%Al-MSU-S before and after exposure to 20% (v/v) water vapor in N_2 at 800 °C for 5 h. Included in Fig. 11, for comparison, are the corresponding patterns for a MCM-41 mesostructure prepared according to the grafting method of Mokaya (denoted CAH5) and a disordered 10%Al-MCM-41 obtained by the same direct assembly route as MSU-S, except that the 100 °C aging step leading to the formation of zeolite Y seeds was eliminated. Clearly, 10%Al-MSU-S assembled from nanoclustered zeolite Y seeds retained a well-ordered hexagonal structure upon steam treatment. In contrast, the conventional 10%Al-MCM-41 and the Al-grafted CAH5 were almost totally destroyed by steaming. These results are also supported by N_2 sorption isotherms (Fig. 12). The 10%Al-MSU-S retained 90 and 75% of its surface area and pore volume, respectively. In addition to the high steam

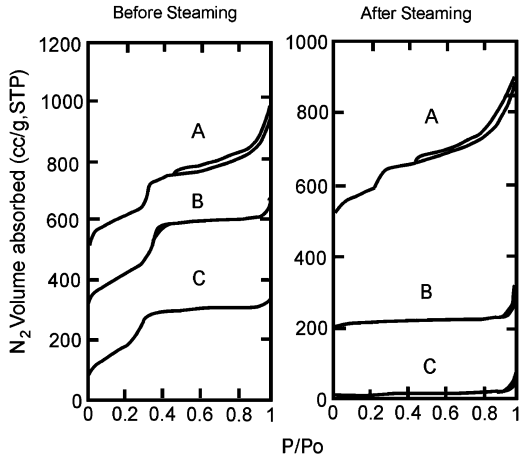

Fig. 12 N_2 adsorption/desorption isotherms for calcined (540 °C, 7 h) mesoporous aluminosilicate molecular sieves before and after steaming (20 vol% H_2O in N_2, 800 °C, 5 h): (A) 10%Al-MSU-S prepared from zeolite Y seeds; (B) "ultrastable" 14%Al-MCM-41 prepared by grafting; (C) 10%Al-MCM-41 prepared by direct synthesis. The isotherms are offset by 200 cc g^{-1} for clarity. Reproduced from ref. 56 by permission of The American Chemical Society.

stability, 10%Al-MSU-S was a far more active acid catalyst for cumene cracking, in comparison to the conventional 10%Al-MCM-41.

Evidence for the presence of zeolite connectivities in Al-MSU-S was provided by the observation of a single tetrahedral aluminum peak at *ca.* 61 ppm in the ^{27}Al NMR spectrum of the calcined mesostructure, which was consistent with the ^{27}Al chemical shift of the zeolite Y seeds solution and the Al environment of crystalline zeolite Y. Normally, a single ^{27}Al NMR peak at a chemical shift near 55 ppm is observed for conventional Al-MCM-41.[68] Also, the dealumination of tetrahedral aluminum in the framework to extra-framework octahedral aluminum occurs during the calcination of conventional MCM-41. However, this scenario was not observed for the calcined Al-MSU-S. Moreover, the chemical shift for the tetrahedral aluminum sites was much larger in Al-MSU-S (61 ppm) than for Al-MCM-41 (55 ppm). Lippmaa *et al.*[69] reported that the chemical shift of tetrahedrally coordinated Al

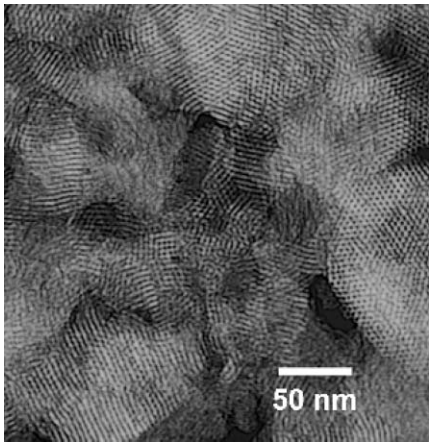

Fig. 13 TEM image of Al-MSU-S (Si/Al = 1.60) prepared from zeolite Y seeds.

centers in zeolites depends on the mean Si–O–Al bond angle in the framework, according to the following linear equation:

$$\delta(\mathrm{Al}) = 0.50\theta - 132 \text{ (ppm)}$$

where δ(Al) is the chemical shift of the Al center, and θ is the mean Si–O–Al bond angle. In general, faujasitic zeolites exhibit chemical shifts higher than 60 ppm because of lower mean Si–O–Al bond angles in the framework in comparison to other zeolites that also contain single and double six-membered ring subunits. The higher chemical shift of the tetrahedral aluminum sites, together the stronger acidity of Al-MSU-S for cumene cracking, implies that zeolite-like connectivities were retained in the Al-MSU-S material.

It should be noted that the occlusion of carbon in the Al-MSU-S framework occurred during the removal of the surfactant upon calcination. It was initially suggested that the steam stability at 800 °C was, in part, a consequence of the exceptional acidity of a framework that formed a small amount of structure-stabilizing carbon (<1 wt%), because removing the carbon lowered the steam stability of the framework. Alternatively, and perhaps more likely, the removal of the embedded carbon induces defects that exposes the framework to attack by water under steaming conditions.

Aside from the improved steam stability and acidity of Al-MSU-S, well-ordered hexagonal Al-MSU-S with an Si/Al ratio as low as 1.6 could be readily assembled from nanoclustered faujasitic seeds. This composition is difficult, if not impossible, to obtain from conventional aluminosilicate precursors. A typical TEM image of such a composition is shown in Fig. 13.

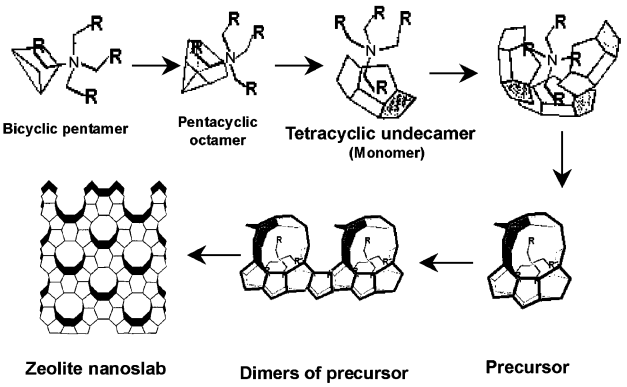

Fig. 14 Proposed nanoclusters[70–73] leading to the nucleation of pentasil nanoslabs.[72,73] Reproduced by permission of The American Chemical Society.

Consequently, nanoclustered zeolite faujasite seeds facilitate the formation of well-ordered hexagonal MCM-41 analogs with higher Al loading.

4.2 Assembly of MCM-41 analogs from high-silica ZSM-5 and Beta zeolite seeds

Following-up on the use of zeolite seeds as precursors for the assembly of steam-stable structures, several workers have used pentasil zeolite seeds, especially BEA and MFI-type seeds.[57–60] In comparison to faujasitic zeolite seeds, which are nucleated by sodium ions, pentasil zeolite seeds are nucleated by specific tetraalkylammonium ions. The structural evolution of nanoclusters leading to the nucleation of MFI silicalite, as shown in Fig. 14, has been studied in detail by van Santen[70] and Martens *et al.*[71–73] Presumably, related structures containing subunits with five-membered rings are encountered before nanoslab formation in pentasil zeolite seed solutions, and these give rise to the characteristic IR-active vibrations between 550–600 cm^{-1}.

In further developing the concept of using protozeolitic nanoclusters for mesostructure assembly, we prepared hydrothermally stable and strongly acidic MCM-41 analogs from zeolite ZSM-5 and Beta seeds, which are nucleated by tetrapropylammonium and tetraethylammonium cations, respectively. The resulting aluminosilicate mesostructures were denoted MSU-$S_{(MFI)}$ and MSU-$S_{(BEA)}$; Table 5 lists the textural properties and cumene cracking activities of MSU-$S_{(MFI)}$ and MSU-$S_{(BEA)}$. For comparison, we include in the table the properties for 1.5%Al-MCM-41, which was prepared by the direct assembly of conventional aluminate and silicate anions.

Table 5 Textural properties and cumene cracking conversions for aluminosilicate molecular sieves. Reproduced from ref. 57 by permission of Wiley-VCH.

Sample	Unit cell dimension a_a/Å	Surface area/m^2 g^{-1}	Pore volume/cm^3 g^{-1}	Pore diameter/Å	Cumene conversion[a] (%)
1.5%Al-MSU-$S_{(MFI)}$					
Calcined	45.3	1231	1.06	36.8	32.3
Steamed 600 °C, 5 h	44.5	1192	0.93	34.7	—
Steamed 800 °C, 5 h	36.6	849	0.44	24.3	—
1.5%Al-MSU-$S_{(BEA)}$					
Calcined	47.3	1124	1.06	39.1	31.5
Steamed 600 °C, 5 h	46.7	1065	0.94	38.0	—
Steamed 800 °C, 5 h	37.0	885	0.46	26.4	—
1.5%Al-MCM-41[b]					
Calcined	46.4	1013	1.08	38.7	11.7
Steamed 600 °C, 5 h	35.2	639	0.39	20.1	—
Steamed 800 °C, 5 h	—	55	—	—	—

[a]Reaction conditions: 6 mm i.d. fixed bed quartz reactor; 200 mg catalyst; cumene flow rate 4.1 μmol min^{-1}; N_2 carrier gas 20 cm^3 min^{-1}; conversions reported after 60 min on-stream at 300 °C. [b]1.5%Al-MCM-41 was prepared by the direct assembly of conventional aluminosilicate anions formed from sodium aluminate, fumed SiO_2, and TMAOH.

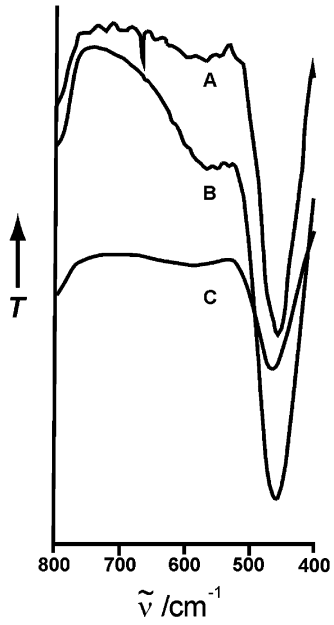

Fig. 15 IR spectra of calcined mesostructures: (A) 1.5%Al-MSU-$S_{(MFI)}$ assembled from zeolite ZSM-5 seeds; (B) 1.5%Al-MSU-$S_{(BEA)}$ assembled from zeolite Beta seeds; (C) 1.5%Al-MCM-41 formed from conventional aluminosilicate precursors. Reproduced from ref. 57 by permission of Wiley-VCH.

For this latter sample the aluminum and silica sources were the same as those used to prepare MSU-$S_{(MFI)}$ and MSU-$S_{(BEA)}$, except that tetramethylammonium hydroxide was used in place of structure-directing tetrapropylammonium or tetraethylammonium hydroxide.

It is clear that both MSU-S aluminosilicate mesostructures undergo little or no degradation after exposure to steam at 600 °C; at least 95% of the surface area and 87% of the pore volume are retained, with no pore contraction. In contrast, 1.5%Al-MCM-41 retained only 63% of the surface area and 36% of the pore volume and experienced an 11 Å pore contraction under equivalent hydrothermal conditions. Upon steaming at 800 °C, the MSU-S analogs still retained long-range hexagonal order and substantial mesoporosity, whereas the mesoporosity of Al-MCM-41 was totally destroyed. Moreover, MSU-$S_{(MFI)}$ and MSU-$S_{(BEA)}$ were far more active acid catalysts than Al-MCM-41 for cumene conversion. These results, together with the improved steam stability, suggest that MSU-$S_{(MFI)}$ and MSU-$S_{(BEA)}$ may be suitable catalysts for the processing of high molecular weight petroleum fractions which can not be adequately refined over microporous zeolite.

We proposed that the hydrothermal stability and catalytic activity of MSU-$S_{(MFI)}$ and MSU-$S_{(BEA)}$ arise form the presence of zeolitic subunits of AlO_4 and SiO_4 tetrahedra in the framework walls of the mesostructures. Evidence for the retention of a protozeolitic connectivity of tetrahedra was provided by IR spectroscopy (Fig. 15). A band characteristic of five-membered ring subunits is apparent in the FTIR spectra of MSU-$S_{(MFI)}$ and MSU-$S_{(BEA)}$, at 550–600 cm^{-1}, but not for conventional Al-MCM-41. Moreover, in accord with the high hydrothermal stability, the ^{29}Si MAS NMR spectra indicated that the framework walls of 2%Al-MSU-S were essentially fully condensed in comparison to 2%Al-MCM-41. As shown in Fig. 16, only one line at −114 ppm (Q^4) was found in the spectrum of 2%Al-MSU-S, whereas two well-resolved lines at −114 (Q^4) and −104 (Q^3) ppm were observed in the spectrum for 2%Al-MCM-41. The high Q^4 intensity for 2%Al-MSU-S signifies the presence of highly crosslinked framework walls.

Zhang *et al.*[59,60] have also reported a hydrothermally stable MCM-41 analog (denoted MAS-5) which was assembled from

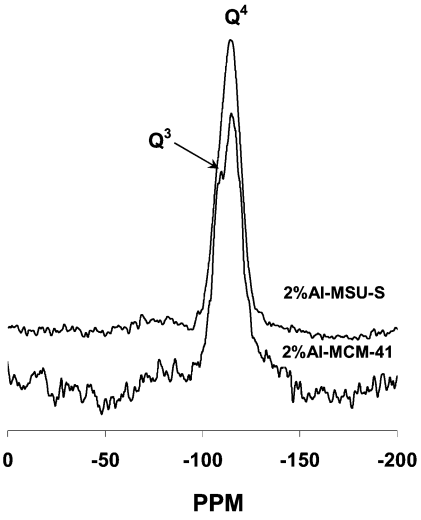

Fig. 16 Comparison of ^{29}Si MAS NMR spectra for calcined 2%Al-MSU-S_{BEA} prepared from zeolite Beta seeds and for calcined 2%Al-MCM-41.

zeolite Beta seeds. Fig. 17 illustrates the XRD patterns of MAS-5 after different hydrothermal treatments. Apparently, MAS-5 still retained well-ordered hexagonal arrays after boiling in water for 300 h or steaming at 800 °C for 2 h. The MAS-5 material also exhibited stronger acidity than conventional Al-MCM-41 for 1,3,5-triisopropylbenzene cracking. In addition, MAS-5 showed higher catalytic activity than Beta zeolite for the alkylation of 2-butene with isobutene (Fig. 18). The acidity of MAS-5 was reported to be very similar to Beta zeolite, as judged by temperature programmed desorption of ammonia (see Fig. 19). The higher catalytic activity for the alkylation was attributed to the easier diffusion of products in the mesoporous channels of MAS-5 than in microporous Beta zeolite. Five-membered ring vibrations also were observed in MAS-5 by IR, which indicated the incorporation of Beta zeolite subunits in the framework.

It should be pointed out that no zeolite phases were observed for MSU-$S_{(MFI)}$, MSU-$S_{(BEA)}$, and MAS-5. These materials should be distinguished from microporous/mesoporous composites. The acidity and hydrothermal stability are attributed to the incorporation of pentasil zeolite subunits into the framework walls of the resultant mesostructures.

4.3 Assembly and grafting of mesostructured cellular foams (MCF) and SBA-15 analogs using zeolite seeds

Unlike MCM-41 mesostructures, which are assembled under basic pH conditions compatible with zeolite seeds, hexagonal SBA-15 and mesostructured cellular foams (MCF) are substantially larger pore (7–35 nm) mesostructures that are normally assembled under strongly acidic conditions. However, sodium silicate can be used as a silica source in place of TEOS to prepare analogous MSU-H and MSU-F mesostructures at a much less acidic pH (*ca.* 5–7).[74] The latter analogs assembled under mildly acidic conditions are not substantially different in structure from the SBA-15 and MCF mesostructures made from TEOS at pH < 2.

In an effort to assemble larger pore SBA-15 and MCF analogs with improved hydrothermal stability and acidity, we have examined the possibility of using nanoclustered faujasite, ZSM-5, and Beta seeds as precursors under mildly acidic pH conditions. The resulting large-pore hexagonal and foam-like MSU-S materials exhibited exceptional hydrothermal stability in boiling water and under steaming conditions.[58] Foam-like MSU-S/F_{FAU}, MSU-S/F_{MFI}, and MSU-S/F_{BEA}, as illustrated in Fig. 20 and Table 6, are much more stable than Al-MCF.

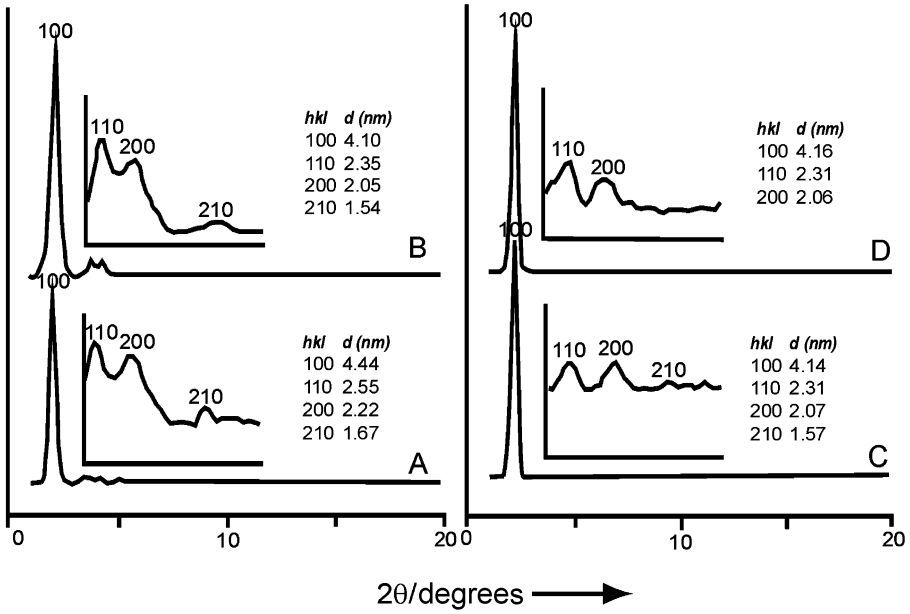

Fig. 17 XRD patterns of (A) as-synthesized MAS-5, (B) MAS-5 calcined at 550 °C for 4 h, (C) calcined MAS-5 after treatment with 100% water vapor at 600 °C for 4 h, and (D) calcined MAS-5 after treatment with 100% water vapor at 800 °C for 2 h. Reproduced from ref. 59 and 60 by permission of Wiley-VCH.

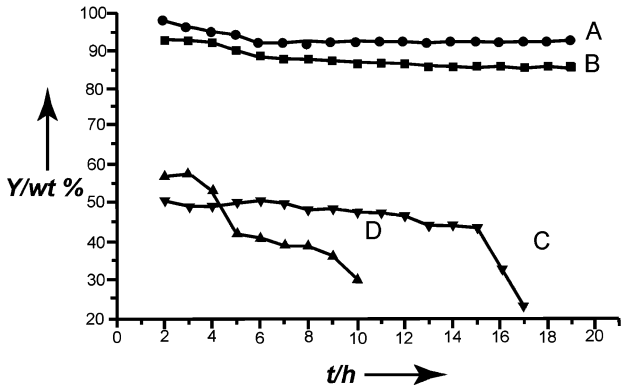

Fig. 18 Catalytic conversion (wt%) *versus* reaction time of 2-butene in the alkylation of isobutane with butene over aluminosilicate catalysts: (A) MAS-5; (B) H-Beta; (C) MCM-41; (D) H-ZSM-5. Reaction temperature 25 °C; isobutane : butane ratio 12 : 1; 1-butene : 2-butene ratio 8 : 1; WHSV (weight hourly space velocity) = 9 h^{-1}. Reproduced from ref. 59 and 60 by permission of Wiley-VCH.

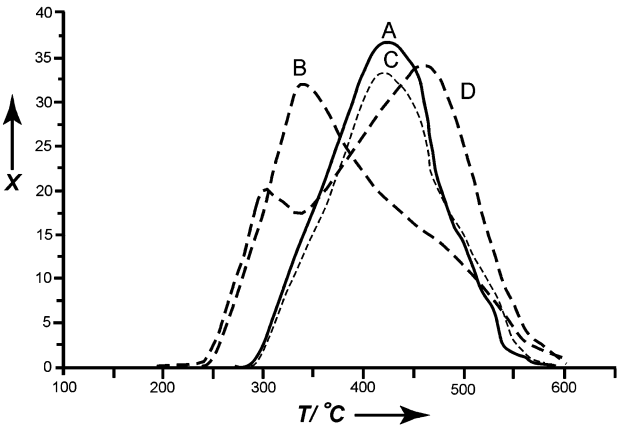

Fig. 19 NH_3-TPD curves for (A) MAS-5, (B) MCM-41, (C) H-Beta, and (D) H-ZSM-5. *X* is the amount of desorbed NH_3. Reproduced from ref. 59 and 60 by permission of Wiley-VCH.

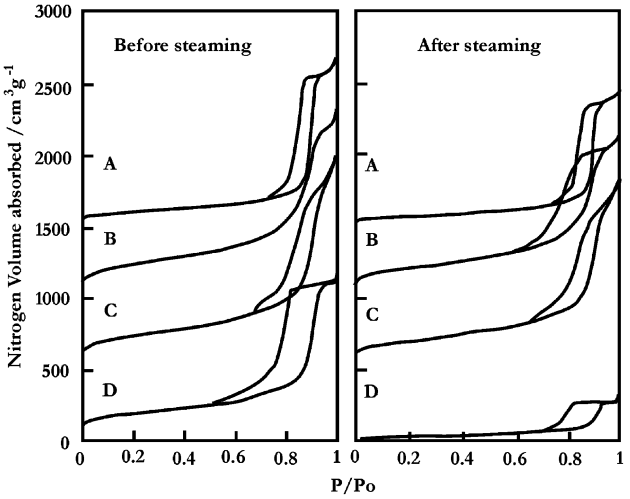

Fig. 20 N_2 isotherms for mesostructured aluminosilicate foams before and after exposure to 20% steam in nitrogen at 800 °C for 2 h: (A) MSU-S/F_{FAU}; (B) MSU-S/F_{MFI}; (C) MSU-S/F_{BEA}; (D) Al-MCF. Each isotherm is offset by 500 cm^3 g^{-1}. Reproduced from ref. 58 by permission of The American Chemical Society.

The MSU-S/F_{BEA} foam, assembled from Beta seeds, exhibited the highest hydrothermal stability. Little structural degradation was observed for MSU-S/F_{BEA} after boiling in water for 250 h and steaming at 800 °C for 2 h.

Evidence for the retention of foam structures was provided by the TEM images shown in Fig. 21. Consistent with the structural features of MCF reported by Stucky's group,[36–39] the MSU-S/F foams are comprised of large spherical cells interconnected by narrow windows defined by aluminosilicate struts. The struts are 4–6 nm in thickness, which is larger than the anticipated size of nanoclustered zeolite seeds.

Although MSU-S/F foam structures were assembled at a pH of 2.5–6, the calcined samples still retained >80% of the aluminum in the tetrahedral positions in the framework walls (Fig. 22), indicating the retention of an acidic framework. In contrast, calcined forms of Al-MCF have essentially all of the aluminum centers in octahedrally coordinated sites, indicating framework walls with poor acidity.

Table 6 Textural properties of calcined mesostructured aluminosilicate foams (Si/Al = 50) before and after hydrothermal stability tests. Reproduced from ref. 58 by permission of The American Chemical Society

Sample	Window size/Å	Cell size/Å	Surface area/ $m^2\ g^{-1}$	Pore vol./ cc g^{-1}	Cumene conv. (%)
MSU-S/F_{FAU}					
Before steaming	132	208	570	1.79	33
After steaming	126	204	462	1.46	
Boiling H_2O	118	196	273	0.78	
MSU-S/F_{MFI}					
Before steaming	102	201	888	1.95	35
After steaming	95	195	748	1.68	
Boiling H_2O	90	187	463	0.96	
MSU-S/F_{BEA}					
Before steaming	128	220	861	2.18	36
After steaming	124	215	737	1.86	
Boiling H_2O	117	210	647	1.87	
MCF					
Before steaming	110	228	715	1.79	<2
After steaming	105	220	147	0.44	
Boiling H_2O	—	—	103	—	

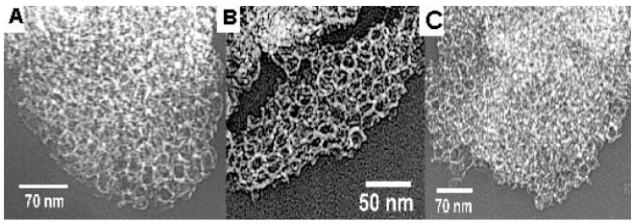

Fig. 21 TEM images of (A) MSU-S/F_{FAU}, (B) MSU-S/F_{MFI}, and (C) MSU-S/F_{BEA}.

Table 7 reports the properties of large pore hexagonal MSU-S/H_{FAU}, MSU-S/H_{MFI}, and MSU-S/H_{BEA} assembled from faujasitic, MFI, and BEA zeolite seeds, respectively, at a pH of *ca.* 5–7. As shown in Table 7, after exposure to steam at 800 °C for 2 h, MSU-S/H_{FAU} retained >65% of its initial surface area and pore volume. MSU-S/H_{MFI} and MSU-S/H_{BEA} are even more stable to steam, retaining >80% of their initial surface areas and pore volumes, with little pore contraction. In contrast, Al-SBA-15 retained only 35% of its initial surface area and pore volume, with substantial pore contraction. In addition to the improved hydrothermal stability, the large pore hexagonal and foam-like MSU-S materials all exhibited higher cumene cracking activities than the corresponding Al-MCF and Al-SBA-15 analogs (Tables 6 and 7).

Most recently, Han *et al.*[61] reported that a hydrothermally stable SBA-15 analog (denoted MAS-9) can be assembled from ZSM-5 seeds. As shown in Table 8, MAS-9 exhibited better hydrothermal stability in boiling water and stronger acidity for hydrocarbon conversion.

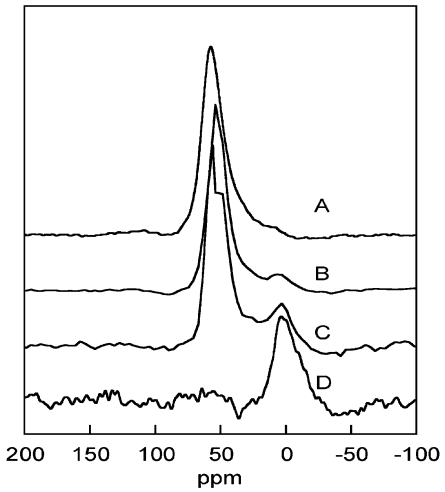

Fig. 22 ^{27}Al MAS NMR spectra of (A) MSU-S/F_{FAU}, (B) MSU-S/F_{MFI}, (C) MSU-S/F_{BEA}, and (D) Al-MCF.

In more recent work, an interesting extension of the use of zeolite seeds to prepare hydrothermally stable and strongly acidic mesostructures as grafting sources was reported by Kaliaguine *et al.*[75] A clear ZSM-5 seed solution was used to graft the seeds onto the framework walls of a primary Al-SBA-15 at 130 °C for 24 h. The resultant SBA-15 analog (denoted ZC MeosAS) exhibited much improved hydrothermal stability. As illustrated in Table 9, even after steaming at 800 °C for 24 h, ZC MesoAs still retained its structural integrity. The increase in Brønsted acid sites in ZC MesoAs in comparison to the parent Al-SBA-15 was provided by FTIR (Fig. 23). The order of acidic strength was H-ZSM-5 > ZC MesoAS > parent Al-SBA-15.

The increased hydrothermal stability and acidity of ZC MesoAS were attributed to the coating of nanosized ZSM-5 seeds on the walls of the parent SBA-15. Evidence for nanosized zeolite seeds coated on the framework walls was provided by IR spectra, which exhibited a vibration band at 550–600 cm^{-1}. As stated above, this band arises from the five-membered ring of vibrations of pentasil zeolite building subunits. Also, a higher Q^4/Q^3 ratio was observed in ZC MesoAS in comparison to the parent SBA-15, which reflected the transformation of the hydrophilic surface of the parent SBA-5 into a more hydrophobic one upon seed grafting. This successful use of zeolite seeds as a grafting reagent to generate

Table 7 Textural properties of calcined large pore hexagonal mesostructured aluminosilicates (Si/Al = 50) before and after hydrothermal stability tests. Reproduced from ref. 58 by permission of The American Chemical Society

Sample	Surface area/ $m^2\ g^{-1}$	*d* Spacing/Å	Unit cell size[a]/Å	Pore size/Å	Pore volume/ $cm^3\ g^{-1}$	Cumene conv. (%)
MSU-S/H_{MFI}						
Before steaming	886	102	118	77	0.93	37
After steaming	701	95	110	69	0.78	
MSU-S/H_{BEA}						
Before steaming	849	101	117	76	0.90	34
After steaming	687	96	111	70	0.77	
MSU-S/H_{FAU}						
Before steaming	653	110	127	90	0.85	32
After steaming	421	95	110	80	0.57	
SBA-15						
Before steaming	823	101	117	77	0.89	2
After steaming	305	86	96	60	0.31	

[a]Unit cell size was calculate from the relationship $a = 2d_{100}/\sqrt{3}$.

Table 8 Properties and cracking activites for cumene and 1,3,5-triisopropylbenzene of various samples before and after treatment in boiling water for 120 h.[a] Reproduced from ref. 61 by permission of The American Chemical Society

Sample	d_{100}/Å	Pore size/Å	Wall thickness/Å	Micropore vol./ $cm^3\ g^{-1}$	Surface area/ $m^2\ g^{-1}$	Cumene conversion (%)	1,3,5-Triisopropylbenzene conversion (%)
MAS-9							
Before treatment	116	80	54	0.16	967	41.5	92.4
After treatment	121	96	43	0.08	680	12.7	34.6
SBA-15							
Before treatment	95	76	34	0.05	910	Inactive	Inactive
After treatment				0	98	Inactive	Inactive
Al-SBA-15[b]							
Before treatment					924	7.8	36.5
After treatment					85	<2.0	<5.0
Al-SBA-15[c]							
Before treatment					1025	25.5	52.4
After treatment					167	<2.0	<5.0
HZSM-5						94.4	1.7

[a]The Si/Al ratio in all samples is 40, except for SBA-15 (pure silica). The MAS-9 sample and the SAB-15 sample were prepared under the same conditions. Pore size distributions and pore volume were determined from N_2 adsorption isotherms at 77 K. The wall thickness was calculated as a_o − pore size ($a_o = 2d_{100}/\sqrt{3}$). [b]Al-SBA-15 prepared by the grafting method. [c]Al-SBA-15 prepared according to the method reported in ref 68.

Table 9 Physicochemical properties of the parent mesoporous aluminosilicates (PMesoAS) and ZSM-5-coated mesoporous aluminosilicates (ZCMesoAS) samples before and after hydrothermal treatments. Reproduced from ref. 75 by permission of Wiley-VCH

Material	Treatment time/h	S_{BET}/ $m^2\ g^{-1}$	Mesopore volume/ $cm^3\ g^{-1}$	BJH pore diameter/Å
Boiling water at 100 °C				
PMesoAS-0-W[a]	0	1080	1.56	70
PMesoAS-48-W	48	415	1.72	120
ZCMesoAS-0-W	0	495	0.78	52
ZCMesoAS-48-W	48	475	0.85	55
ZCMesoAS-120 W	20	485	1.35	58
Steaming in 20% water in N_2 at 800 °C				
ZCMesoAS-24-S	24	445	0.70	53

[a]For the designation PMesoAS-*x*-W or S, *x* is the treatment time in hours; W denotes boiling water and S denotes steam treatment.

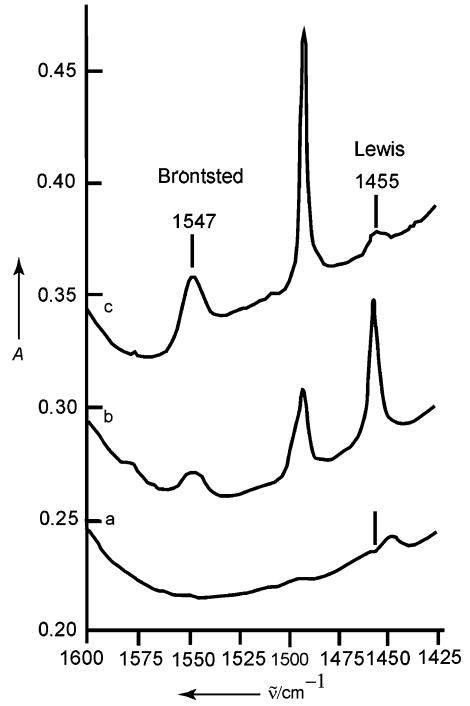

Fig. 23 FTIR spectra of adsorbed pyridine in the 1350–1600 cm^{-1} range after pyridine was adsorbed and then desorbed at 150 °C: (a) parent MesoAS in H-form; (b) ZSM-5-coated MesoAS; (c) H-ZSM-5. Reproduced from ref. 75 by permission of Wiley-VCH.

steam-stable and strongly acidic mesostructures goes beyond the previous routes using pure aluminum salts as grafting agents.

5 Summary and outlook

A decade has passed since the exciting discovery of MCM-41 by Mobil scientists. To overcome the drawbacks of mesoporous aluminosilicates in comparison to microporous crystalline zeolite, much effort has been made in the synthesis of these materials to improve their hydrothermal stability and acidity. Through the creative use of new surfactants and novel reaction conditions, thicker wall mesoporous silica mesostructures, such as hexagonal SBA-15 and lamellar MSU-G, have been assembled. The post-synthesis grafting of aluminum salts onto the thicker wall mesostructures, along with the partial conversion of the framework walls into nanosized zeolite phases, have lead to compositions with acidities and hydrothermal stabilities that go far beyond those of the original M41S materials. The most significant improvement in both the acidity and the hydrothermal stability of aluminosilicate mesostructures, however, comes through the use of nanoclustered zeolite seeds as precursors for direct assembly and as post-assembly grafting reagents. These materials are potential catalysts for large molecule conversions, especially the processing of petroleum distillates that are too large to crack with conventional zeolite catalysts. Also, the use of protozeolitic nanoclusters for the preparation of improved mesostructures is not limited to aluminosilicates. Metal-substituted seed compositions, such as those used to nucleate zeolite-like TS-1, Ga-MFI, and AlPO, among other microporous molecular sieve structures, may be advantageous precursors for the preparation of stable mesostructures.[76] Finally, there is probably little risk in predicting that a mesostructured aluminosilicate with fully crystalline walls will be developed in the future. Recently, an ordered mesoporous organosilica hybrid material with crystal-like framework walls was successfully synthesized by Inagaki *et al.*[77] This successful example, along with recent examples of molecular order in surfactant-templated lamellar silicates,[78] should encourage researchers to pursue the ultimate goal of designing aluminosilicate mesostructures with atomically ordered walls.

Acknowledgement

The support of the National Science Foundation under CRG grants CHE-9903706 and CHE-0211029 is greatly appreciated.

References

1 C. T. Kresge, M. E. Leonowicz, W. J. Roth, J. C. Vartuli and J. S. Beck, *Nature*, 1992, **359**, 710–712.
2 J. S. Beck, D. C. Calabro, S. B. McCullen, B. P. Pelrine, K. D. Schmitt and J. C. Vartuli, *US Pat.*, 5,200,058 and 5,220,101, 1993.
3 J. S. Beck, *US Pat.*, 5,057,296, 1991.
4 C. T. Kresge, M. E. Leonowicz, W. J. Roth and J. C. Vartuli, *US Pat.*, 5,098,684, 1992.
5 J. S. Beck, C. T. W. Chu, I. D. Johnson and C. T. Kresge, *WO Pat.*, 91/11390, 1991.
6 J. S. Beck and J. C. Vartuli, *Curr. Opin. Solid State Mater. Sci.*, 1996, **1**, 76–87.
7 J. S. Beck, J. C. Vartuli, G. J. Kennedy, C. T. Kresge, W. J. Roth and S. E. Schramm, *Chem. Mater.*, 1994, **6**, 1816–1821.
8 J. S. Beck, J. C. Vartuli, W. J. Roth, M. E. Leonowicz, C. T. Kresge, K. D. Schmitt, C. T. W. Chu, D. H. Olson, E. W. Sheppard, S. B. McCullen, J. B. Higgins and J. L. Schlenker, *J. Am. Chem. Soc.*, 1992, **114**, 10834–10843.
9 J. M. Kim, S. K. Kim and R. Ryoo, *Chem. Commun.*, 1998, 259–260.
10 A. Sayari, *J. Am. Chem. Soc.*, 2000, **122**, 6504–6505.
11 Y. Liu, A. Karkamkar and T. J. Pinnavaia, *Chem. Commun.*, 2001, 1822–1823.
12 P. T. Tanev, M. Chibwe and T. J. Pinnavaia, *Nature*, 1994, **368**, 321–323.
13 P. T. Tanev, Y. Liang and T. J. Pinnavaia, *J. Am. Chem. Soc.*, 1997, **119**, 8616–8624.
14 P. T. Tanev and T. J. Pinnavaia, *Supramol. Sci.*, 1998, **5**, 399–404.
15 P. T. Tanev and T. J. Pinnavaia, *Chem. Mater.*, 1996, **8**, 2068–2079.
16 P. T. Tanev and T. J. Pinnavaia, *Science*, 1996, **271**, 1267–1269.
17 P. T. Tanev and T. J. Pinnavaia, *Science*, 1995, **267**, 865–867.
18 P. T. Tanev and T. J. Pinnavaia, *Access Nanoporous Mater., [Proc. Symp.]*, 1995, 13–27.
19 P. T. Tanev and T. J. Pinnavaia, *Mater. Res. Soc. Symp. Proc.*, 1995, **371**, 63–67.
20 S. A. Bagshaw, T. Kemmitt and N. B. Milestone, *Microporous Mesoporous Mater.*, 1998, **22**, 419–433.
21 S. A. Bagshaw and T. J. Pinnavaia, *Angew. Chem., Int. Ed. Engl.*, 1996, **35**, 1102–1105.
22 S. A. Bagshaw, E. Prouzet and T. J. Pinnavaia, *Science*, 1995, **269**, 1242–1244.
23 S. A. Bagshaw, *Mesoporous Molecular Sieves 1998*, 1998, **117**, 381–389.
24 W. Zhang, T. R. Pauly and T. J. Pinnavaia, *Chem. Mater.*, 1997, **9**, 2491–2498.
25 T. R. Pauly, Y. Liu and T. J. Pinnavaia, in *Book of Abstracts, 219th ACS National Meeting, San Francisco, CA, March 26-30, 2000*, American Chemical Society, Washington, DC, 2000, CATL-025.
26 T. R. Pauly, Y. Liu, T. J. Pinnavaia, S. J. L. Billinge and T. P. Rieker, *J. Am. Chem. Soc.*, 1999, **121**, 8835–8842.
27 T. R. Pauly and T. J. Pinnavaia, *Chem. Mater.*, 2001, **13**, 987–993.
28 S. S. Kim, W. Z. Zhang and T. J. Pinnavaia, *Science*, 1998, **282**, 1302–1305.
29 S. S. Kim, Y. Liu and T. J. Pinnavaia, *Microporous Mesoporous Mater.*, 2001, **44**, 489–498.
30 D. Zhao, J. Feng, Q. Huo, N. Melosh, G. H. Frederickson, B. F. Chmelka and G. D. Stucky, *Science*, 1998, **279**, 548–552.
31 D. Zhao, Q. Huo, J. Feng, B. F. Chmelka and G. D. Stucky, in *Book of Abstracts, 214th ACS National Meeting, Las Vegas, NV, September 7-11, 1997*, American Chemical Society, Washington, DC, 1997, PHYS-373.
32 D. Zhao, Q. Huo, J. Feng, B. F. Chmelka and G. D. Stucky, *J. Am. Chem. Soc.*, 1998, **120**, 6024–6036.
33 D. Zhao, Q. Huo, J. Feng, J. Kim, Y. Han and G. D. Stucky, *Chem. Mater.*, 1999, **11**, 2668–2672.
34 D. Zhao, J. Sun, Q. Li and G. D. Stucky, *Chem. Mater.*, 2000, **12**, 275–279.
35 S. S. Kim, T. R. Pauly and T. J. Pinnavaia, *Chem. Commun.*, 2000, 1661–1662.
36 P. Schmidt-Winkel, C. J. Glinka and G. D. Stucky, *Langmuir*, 2000, **16**, 356–361.
37 P. Schmidt-Winkel, W. W. Lukens Jr., P. Yang, D. I. Margolese, J. S. Lettow, J. Y. Ying and G. D. Stucky, *Chem. Mater.*, 2000, **12**, 686–696.
38 P. Schmidt-Winkel, W. W. Lukens Jr., D. Zhao, P. Yang, B. F. Chmelka and G. D. Stucky, *Mater. Res. Soc. Symp. Proc.*, 1999, **576**, 241–246.
39 P. Schmidt-Winkel, W. W. Lukens Jr., D. Zhao, P. Yang, B. F. Chmelka and G. D. Stucky, *J. Am. Chem. Soc.*, 1999, **121**, 254–255.
40 A. Corma, M. S. Grande, V. GonzalezAlfaro and A. V. Orchilles, *J. Catal.*, 1996, **159**, 375–382.
41 H. Y. Zhu, G. Q. Lu and X. S. Zhao, *J. Phys. Chem. B*, 1998, **102**, 7371–7376.
42 X. S. Zhao and G. Q. Lu, *J. Phys. Chem. B*, 1998, **102**, 1556–1561.
43 X. S. Zhao, G. Q. Lu and X. Hu, *Microporous Mesoporous Mater.*, 2000, **41**, 37–47.
44 R. Mokaya, *Chem. Commun.*, 1997, 2185–2186.
45 R. Mokaya, *Angew. Chem., Int. Ed.*, 1999, **38**, 2930–2934.
46 R. Mokaya, *J. Phys. Chem. B*, 1999, **103**, 10204–10208.
47 R. Mokaya, *Adv. Mater.*, 2000, **12**, 1681–1685.
48 R. Mokaya, *Chem.Commun.*, 2001, 933–934.
49 R. Mokaya, *Chem. Commun.*, 2001, 633–634.
50 J. M. Kim, S. Jun and R. Ryoo, *J. Phys. Chem. B*, 1999, **103**, 6200–6205.
51 D. T. On, P. Reinert, L. Bonneviot and S. Kaliaguine, *Stud. Surf. Sci. Catal.*, 2001, **135**, 929–937.
52 D. T. On and S. Kaliaguine, *Angew. Chem., Int. Ed. Engl.*, 2001, **40**, 3248–3251.
53 L. Huang, W. Guo, P. Deng, Z. Xue and Q. Li, *J. Phys. Chem. B*, 2000, **104**, 2817–2823.
54 L. Huang and Q. Li, *Proc. Int. Zeolite Conf., 12th*, 1999, **1**, 707–712.
55 K. R. Kloetstra, H. W. Zandbergen, J. C. Jansen and H. Van Bekkum, *Chem. Ind. (Dekker)*, 1998, **74**, 159–174.
56 Y. Liu, W. Zhang and T. J. Pinnavaia, *J. Am. Chem. Soc.*, 2000, **122**, 8791–8792.
57 Y. Liu, W. Zhang and T. J. Pinnavaia, *Angew. Chem., Int. Ed.*, 2001, **40**, 1255–1258.
58 Y. Liu and T. J. Pinnavaia, *Chem. Mater.*, 2002, **14**, 3–5.
59 Z. T. Zhang, Y. Han, F. S. Xiao, S. L. Qiu, L. Zhu, R. W. Wang, Y. Yu, Z. Zhang, B. S. Zou, Y. Q. Wang, H. P. Sun, D. Y. Zhao and Y. Wei, *J. Am. Chem. Soc.*, 2001, **123**, 5014–5021.
60 Z. T. Zhang, Y. Han, L. Zhu, R. W. Wang, Y. Yu, S. L. Qiu, D. Y. Zhao and F. S. Xiao, *Angew. Chem., Int. Ed.*, 2001, **40**, 1258–1253.
61 Y. Han, S. Wu, Y. Sun, D. Li, F.-S. Xiao, J. Liu and X. Zhang, *Chem. Mater.*, 2002, **14**, 1144–1148.
62 Y. H. Yue, A. Gedeon, J. L. Bonardet, N. Melosh, J. B. D'Espinose and J. Fraissard, *Chem. Commun.*, 1999, 1967–1968.
63 R. Mokaya, W. Zhou and W. Jones, *Chem. Commun.*, 1999, 51–52.
64 T. R. Pauly, V. Petkov, Y. Liu, S. J. L. Billinge and T. J. Pinnavaia, *J. Am. Chem. Soc.*, 2002, **124**, 97–103.
65 K. Richard Kloetstra, J. C. Jansen and H. van Bekkum, *Chem. Commun.*, 1997, 2281–2282.
66 M. J. Verhoef, P. J. Kooyman, J. C. van der Waal, M. S. Rigutto, J. A. Peters and H. van Bekkum, *Chem. Mater.*, 2001, **13**, 683–687.
67 D. Trong On, D. Lutic and S. Kaliaguine, *Microporous Mesoporous Mater.*, 2001, **44–45**, 435–444.
68 R. B. Borade and A. Clearfield, *Catal. Lett.*, 1995, **31**, 267–272.
69 E. Lippmaa, A. Samoson and M. Magi, *J. Am. Chem. Soc.*, 1986, **108**, 1730–1735.
70 P. E. A. de Moor, T. P. M. Beelen and R. A. Van Santen, *J. Phys. Chem. B*, 1999, **103**, 1639.
71 C. E. A. Kirschhock, R. Ravishankar, P. A. Jacobs and J. A. Martens, *J. Phys. Chem. B*, 1999, **103**, 11021–11027.
72 C. E. A. Kirschhock, R. Ravishankar, L. Van Looveren, P. A. Jacobs and J. A. Martens, *J. Phys. Chem. B*, 1999, **103**, 4972–4978.
73 C. E. A. Kirschhock, R. Ravishankar, F. Verspeurt, P. J. Grobet, P. A. Jacobs and J. A. Martens, *J. Phys. Chem .B*, 1999, **103**, 4965–4971.
74 S. S. Kim, A. Karkamkar, T. J. Pinnavaia, M. Kruk and M. Jaroniec, *J. Phys. Chem. B*, 2001, **105**, 7663–7670.
75 D. T. On and S. Kaliaguine, *Angew. Chem., Int. Ed.*, 2002, **41**, 1036–1040.
76 F.-S. Xiao, Y. Han, Y. Yu, X. Meng, M. Yang and S. Wu, *J. Am. Chem. Soc.*, 2002, **124**, 888–889.
77 S. Inagaki, S. Guan, T. Ohsuna and O. Terasaki, *Nature*, 2002, **416**, 304–307.
78 S. C. Christiansen, D. Zhao, M. T. Janicke, C. C. Landry, G. D. Stucky and B. F. Chmelka, *J. Am. Chem. Soc.*, 2001, **123**, 4519–4529.